Fuel 253 (2019) 1414–1423

Contents lists available at ScienceDirect

Fuel

journal homepage: www.elsevier.com/locate/fuel

Full Length Article

Measurement and characterization of biomass mean residence time in an air-blown bubbling fluidized bed gasification reactor

Cornelius E. Agu[a,*], Christoph Pfeifer[b], Marianne Eikeland[a], Lars-Andre Tokheim[a], Britt M.E. Moldestad[a]

[a] Department of Process, Energy and Environmental Technology, University of South-Eastern Norway, 3918 Porsgrunn, Norway
[b] Department of Material Sciences and Process Engineering, University of Natural Resources and Life Sciences, 1190 Vienna, Austria

ARTICLE INFO

Keywords:
Biomass gasification
Residence time
Char accumulation
Bubbling bed
Devolatilization

ABSTRACT

Gasification of biomass in bubbling fluidized beds can be limited by accumulation of unconverted char particles during the process. The amount of unconverted biomass depends on the residence time of the fuel particles. This study demonstrates a method for measuring the biomass residence time over the conversion period at a given air flowrate and a given amount of biomass in a bubbling bed using the variation of bed temperature and fluid pressure recorded over time. The results show that biomass conversion is characterized by the devolatilization and extinction times. The two biomass residence times increase with decreasing air flowrate and increasing amount of biomass charged in the bed. The amount of unconverted char between the two characteristic times also increases with decreasing air flowrate and increasing biomass load. The total heat loss during the devolatilization is observed to increase with increasing air flowrate and amount of biomass in the bed. Correlations are proposed for predicting the mean biomass residence time, the amount of unconverted char particles and the devolatilization heat loss at a given operating condition. The results of this study can be used in determining the bubbling bed properties and solid circulation rate required to decongest the accumulated char particles in the bed.

1. Introduction

Fluidized bed reactors can be operated under bubbling or circulating bed regimes for chemical conversion and synthesis. In biomass gasification for example, a combination of these regimes in so-called dual-fluidized bed reactors can be used to ensure efficient utilization of the carbon content of the fuel particles [1]. However, application of a single bubbling or circulating bed reactor offers simpler process design and depending on the utilization route of the producer gas, the type of reactor has to be chosen. In a fluidized bed reactor, an inert bed material is used to aid the fluidization quality of biomass, which is usually difficult to fluidize due to its peculiar shape, size and cohesiveness. Bed fluidization helps to achieve uniform material and heat distribution, thereby enhancing the reaction rates in the reactor. The fluidization also influences the residence time distribution [2,3] and the conversion efficiency of the fuel particles [4]. In addition, the distribution of biomass in a fluidized bed depends on a number of factors including the biomass type, gas velocity and reactor design.

There are different studies on biomass residence time in fluidized beds. The definition of the particle residence times covered in literature depends on the purpose and thus must be clear for its application. The biomass residence time can be determined on the basis of its transport time between two reference positions in the bed, on the basis of the relative amount participating in reactions and on the basis of the time elapsed before complete conversion of the particles has been achieved. Although the later definition is implied in this study, the different types of biomass residence time are interrelated. The fuel conversion time may be longer if it does not receive adequate heat and gasification agent within the bed. The biomass particles can be transported to the surface or bottom of the bed due to segregation effect [5], and thus have limited contact time with the bed material supposed to provide the heat required for the reaction. The particle segregation can be brought about by the density difference between biomass and the bed material particles [6], and by the rise of gas bubbles formed around the particles as biomass undergoes devolatilization [7,8]. The mean residence time and residence time distribution characterize the degree of mixing in a non-catalytic fluidized bed reactor [9]. Gao et al. [10] concluded that the particle flow pattern in a bubbling fluidized bed lies between those

* Corresponding author.
E-mail addresses: cornelius.e.agu@usn.no, agumech@yahoo.com (C.E. Agu), christoph.pfeifer@boku.ac.at (C. Pfeifer), Marianne.Eikeland@usn.no (M. Eikeland), Lars.A.Tokheim@usn.no (L.-A. Tokheim), britt.moldestad@usn.no (B.M.E. Moldestad).

https://doi.org/10.1016/j.fuel.2019.05.103
Received 18 January 2019; Received in revised form 22 April 2019; Accepted 21 May 2019
Available online 29 May 2019

Nomenclature

Symbols

A [m^2]	cross-sectional area
a [−]	dimensionless fitting parameter
D [m]	bed diameter
d [m]	particle diameter
h_0 [m]	initial bed height
m [kg]	mass
$\dot{m}$ [kg/s]	mass flowrate
p [Pa]	fluid pressure
$\dot{q}_L$ [K/s]	heat loss
T [K]	temperature
t [s]	time
t_* [s]	mean residence time
U [m/s]	superficial air velocity
x [−]	solid fuel to bed material mass ratio
y_{char} [−]	char mass fraction in a bed
Y [−]	volume fraction of solid component

Greek letters

α [−]	degree of conversion completeness
ε [−]	void fraction of bulk material
ρ [kg/m^3]	density
σ	standard deviation
φ [−]	particle sphericity
γ_{char} [−]	characteristic fraction of unconverted char particles

Subscripts

b	biomass
c	complete
p	particle/pressure
mf	minimum fluidization
s	sand
0	initial/bottom reference

of the ideal plug flow and perfectly stirred reactor. Zou et al. [2] showed that an increase in the feed rate of solid particles makes the solids flow pattern closer to plug flow. As reported in different studies, different factors influence the residence time of biomass in fluidized beds. An increase in gas velocity and bed height leads to a wider residence time distribution of solid particles [2]. Larger particles have longer mean residence time [2,3] and lower descending vertical velocity [2]. The mean residence time of solid particles also increases with increasing bed height and decreasing gas velocity in bubbling beds [3].

In addition to distribution of biomass particles, the amount of biomass residing in the bed at a given operating condition determines its conversion efficiency. The conversion efficiency can be measured by the relative flow of carbon entering as solid and leaving the reactor as gas [4]. Before being completely converted, char particles can be reduced to elutriable sizes by attrition, fragmentation or both. Particle elutriation reduces the amount of active carbon for efficient conversion. When the elutriation effect is reduced, the char residence time can be longer, increasing the char conversion efficiency due to increased chemical kinetics rates [11–13]. The carbon conversion can be increased by improving the biomass devolatilization process since elutriation of char particles increases with the amount in the bed [14]. Although it is usually believed that devolatilization is a fast process, completing in few seconds depending on the particle size [15], heating rate [16,17] and the final temperature [16–19], Gable and Brown [20] clearly showed that this process can take more than 40 s to be essentially complete. Higher temperature and heating rate will for the same fuel particles result in a higher amount of volatiles and a lower amount of char in the bed. Moreover, a complete conversion of char in a bed may also not be possible due to a number of factors including the deactivation (thermal and graphitization) effect [21–23], competing reactions within the vicinity of the char particles that may result in reducing the availability of the gasifying agent, and the competing rates between the mass transfer and reaction rate.

In addition to thorough studies on the distribution of biomass in fluidized bed reactors, this paper is aimed at presenting the measurement of the total time required for a given type and amount of biomass to be completely converted in a conventional air-blown bubbling fluidized bed reactor, assuming no elutriation of the fuel particles. Before biomass particles are completely converted, they usually undergo different reaction phases such as devolatilization and partial oxidation. By tracking the changes in the reaction phases, the amount of biomass unconverted over time can be determined. The fraction of biomass in a bed under a specific condition is a useful parameter for design purpose. For a mixture of bed material and biomass particles, the prediction of minimum fluidization velocity [24,25], minimum slugging velocity and bed expansion [26] depends on the proportion of biomass in the bed. With the knowledge of rate of accumulation of char particles, the solid circulation rate applicable in dual fluidized bed reactors can also be determined.

For measurement of biomass residence time based on the relative movement of particles in the bed, different techniques are used. The most common of these techniques are based on single particle tracing [3] and on stimulus responses from chemical differences [27], radioactivity measurements [28] or phosphorescence [29]. The char yield during devolatilization is usually obtained by cooling and weighing method for a given measurement condition. By noting that the pressure drop increases linearly with the amount of char in a bubbling bed, Xu et al. [30] applied the measurement of bed pressure drop to determine the char yield at a given temperature under the atmosphere of nitrogen.

In this study, the experiments are conducted in batches in a non-transparent reactor using air as the fluidizing gas. The technique employed involves measurement of fluid pressure and temperature in the bed over a period of time. As the fluid pressure increases upon introducing biomass in the bed, the fractional change in the pressure indicates the amount of biomass consumed. The peak temperature recorded over the conversion period gives an indication about the completeness of the reaction. Due to partial oxidation with the available oxygen, the amount of char obtained in this study may be lower than that obtained when nitrogen is used as the fluidizing gas. However, the measured char yield still stands a chance of representing the true value when using air for biomass conversion. The detailed experimental procedure is presented in the following section. The results of the data obtained at different biomass loads and air flowrates are presented, analysed and discussed in the subsequent sections. The method developed and described here allows a quick and relatively easy determination of biomass conversion characteristics as well as char residence time in fluidized bed without complex and costly measurement procedure. The findings are based on comprehensive measurements under hot-flow conditions, analyses of cold-flow model results and mathematical modelling.

2. Experimental procedures

To gain in-depth understanding of how much time it takes a given amount of biomass to be completely converted at a given air flowrate, a batch process was used. This section presents a brief description of the bubbling fluidized bed reactor used, and also the detailed procedure employed in measuring the biomass residence time over the reaction

period and the amount of unconverted biomass particles as the reaction goes.

2.1. Experimental setup

As shown in Fig. 1, the experimental setup consists of a stainless-steel cylindrical column with 10 cm internal diameter, thickness of 4 mm and height of 1.0 m above the distributor. Three electric heating elements attached externally along the column wall are used to supply heat to the reactor up to 1000 °C. To minimize the heat loss, the inner side of the reactor is coated with a refractory material while the outer part is insulted with 200 mm thick fiberglass. The behaviour in the reactor is monitored with five different thermocouples and five different pressure sensors located along the vertical axis as shown. Each pressure sensor consists of a pressure tube connected to a pressure transducer through a 4 mm flexible tube, and measures the gauge pressure (i.e. the fluid pressure in excess of the atmospheric pressure) in the given location. The fuel supply is through a screw feeder, which is calibrated for each fuel applied. Air is supplied through two 10 mm-steel pipes positioned 27.5 mm from the column base. The mass flow-rate of air is measured with a BROOK air flowmeter (3809 series) operating in the range, 0.48–4.7 kg/h. Above the reactor column, a gas sampling point is installed. The product gas from the reactor is passed through a flare before being discharged to the atmosphere.

In the experiments, compressed air was used as the fluidizing gas and oxygen carrier. Sand particles with mean particle size of 293 μm were used as the bed material. The mass of the bed material maintained throughout the experiments was 2.2 kg. Two different types of woody biomass were used; wood pellets and wood chips. The properties of the biomass and sand particles at the ambient condition are shown in Table 1, where ρ_p is the particle density, d_p the volume-equivalent spherical diameter, φ_p is the particle sphericity and ε is the void fraction of the bulk material. The wood pellets are cylindrical with diameter 6 mm and length in the range 5–30 mm. The wood chips are considered rectangular with variation in length, width and height in the range of 5–12 mm, 5–12 mm and 1–5 mm, respectively. The sand particle size was obtained by sieve analysis and the volume-equivalent spherical diameter of the biomass particles were computed from the particle geometry.

The experiments were conducted in batches using five different biomass loads in the range 90–450 g. The proportion of biomass in the total solid mixture is given in Table 2, where m_b is the initial mass of biomass loaded in the bed, x_b is the mass ratio between biomass and sand particles, and Y_b is the volume percentage of biomass in the total bed mixture. For each biomass load, six different air flowrates in the range 0.5–2 kg/h were used.

It should be noted that in a continuous process, the amount of air supply is related to the biomass feed rate, where for a typical woody biomass, the minimum air–fuel ratio (AFR) to achieve a complete combustion is about 6. To achieve a gasification, AFR$\ll$ 6. In a batch process, the AFR criterion is not applicable since the amount of biomass in the bed decreases with time. However, in addition to minimizing the particle elutriation, the range of air flowrates applied in this study is based on the amounts that promote gasification at the initial stage assuming that the rate of mass loss is constant over the conversion period. As reported in Tran and White [31], the mass loss during conversion of redwood is in the range 2.92–6.25 g/m^{2}s depending on the ignition heat flux. Assuming a value of 3.0 g/m^{2}s, the estimated air–fuel ratio over the range of biomass loads and air flowrates used in this study is within 0.2–1.4, which is in the range applied for a gasification process.

In each experiment, the sand bed was initially heated up at the applied air flowrate using the reactor heater. When the desired temperature 830 ± 20 °C was achieved, the heater was turned off and the required amount of biomass was then loaded. The temperatures and pressures at different bed positions 1–5 were captured at 1 sec intervals. The product gas was also sampled at 5 min intervals for offline analysis using the SRI gas chromatography (GC). The GC uses a TCD detector and helium as carrier gas with an installed column comprising a packed Molecular Sieve 13x. The GC operates at 10 psi in the temperature range −15 to 120 °C, and provides the composition of the major fuel gases: carbon monoxide (CO), hydrogen (H_2) and methane (CH_4) as well as nitrogen and oxygen in each gas sample by the gradient-method. Each experiment was performed twice to confirm the repeatability, and the two data sets were averaged and recorded.

2.2. Measurement of devolatilization and char residence times

Fig. 2 shows the variations of pressure drop measured at the base (position 1) and the temperature measured at the position 2 located 14.3 cm from the base of the bed containing 26.4 vol% wood pellets at 1.0 kg/h air flowrate. These temperature and pressure curves are also similar for all other biomass loads and air flowrates, and thus are described as the characteristic curves for a batch biomass conversion in the pilot plant which is typical for a bubbling bed. As shown in the figure, the bed pressure increases rapidly shortly after the required amount of biomass is introduced at point **A**. The peak pressure marked **O** increases with the amount of biomass charged in the bed. As the biomass undergoes conversion, the pressure first drops rapidly until a point **D**, then gently to point **E** and finally levels off to a value the same as that at the initial state. The rapid drop in pressure to point **D** indicates that most of biomass in the bed has been released as gas due to drying and devolatilization. Fig. 2(b) shows that the devolatilization begins as soon as biomass is introduced in the bed. After point **D**, the mole fraction of CH_4 in addition to that of H_2 becomes insignificant ($< 0.5\%$). At point **D**, the concentration of CO is also very low while the N_2 mole fraction is close to 70%. In addition, the temperature decreases below the initial bed temperature and becomes minimum at point **D**, showing that the biomass devolatilization effectively completes at point **D**. During the devolatilization phase, the temperature first slightly drops below point **O** and then sharply to point **D**. The time variation of temperature within the bed may depend on the biomass load and axial position as shown in Fig. 3.

Beyond point **D**, the temperature increases almost linearly until point **P** owing to oxidation of residual fuel gases and char particles. With further increase in time, the temperature increases but at a lower rate as there are little or no more amount of combustible gases in the

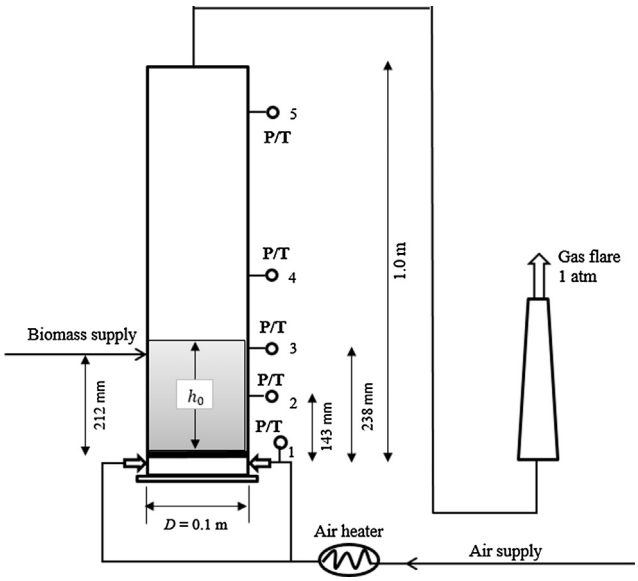

Fig. 1. Schematic illustration of the biomass gasification reactor used for tests. Symbols **P/T** indicate pressure and temperature sensor probes; h_0 is the initial bed height above the air distributor.

Table 1
Biomass and sand particle properties at ambient condition.

Materials	Shape	ρ_p [kg/m^3]	d_p [mm]	φ_p [−]	ε [−]
Wood pellets	Cylindrical	1139	8.96	0.82	0.43
Wood chips	Rectangular	423	6.87	0.75	0.49
Sand	Angular	2650	0.293	0.86	0.42

Table 2
Initial amount and proportion of biomass in the bed solids mixture.

Biomass type	m_b [kg]	x_b [−]	Y_b [vol. %]
Wood pellets	0.230	0.109	20.2
	0.326	0.154	26.4
	0.435	0.206	32.4
Wood chips	0.091	0.043	21.3
	0.156	0.074	31.7

bed. At this stage, the increase in temperature is due to oxidation of char particles in the parts of the bed with available oxygen. When the temperature reaches the peak value at point **E**, almost all the char particles are consumed, resulting in the levelling-off of the pressure in the bed. The temperature decreases beyond point **E** as the heat released from any residual char is significantly lower than the heat loss from the cold air that flows continuously through the bed. As shown in Fig. 3, the temperature is approximately uniform along the reactor after point **E**, suggesting a complete consumption of fuel species in the bed. However, below this point, the figure shows that the temperatures at positions 4 and 5 are higher compared to those in the bed, possibly due to oxidation of fuel gases in the freeboard.

As can be seen in Fig. 2, the biomass conversion process is characterized by two residence times, noted as the devolatilization time, t_d and extinction time, t_e. The devolatilization time is measured at the inflection point on the pressure while the extinction time is measured at the peak of the temperature curve. Within the time interval $[0.t_d]$, the product gas exiting the reactor consists of combustible gases as can be seen in Fig. 2(b). Beyond the time t_d, little or no combustible gas components are present in the exit gas. When the time is increased to the value t_e, the biomass particles are almost completely consumed. The time difference, $(t_e - t_d)$ measures the mean effective char residence time. The mean biomass residence time, t_* can be obtained at the point of intersection between the horizontal line drawn through point **E** and the line of best fit drawn through points **D** and **P** as shown in Fig. 2. The value of t_* is significant when considering a continuous flow process where there is always some amount of unconverted char in the bed.

2.3. Measurement of char yield and heat loss at completion of devolatilization

The peak of the pressure curve is proportional to the amount of biomass charged into the bed at the same air flowrate. The fractional change in the pressure drop as the conversion is going on can thus be used to estimate the change in the amount of biomass consumed in the bed. Between point **D** and **E**, the amount of char released in the bed can be obtained by considering a mass balance across the bed assuming that the pressure drop is related to the amount of solid particles in the bed.

By definition, the char yield γ_{char} at the completion of devolatilization is given by

$$\gamma_{char} = \frac{m_{char}}{m_{bio}} \tag{1}$$

Since the peak pressure drop is proportional to the mass of biomass m_{bio} in the bed, then by the mass balance

$$m_{bio} = \frac{A(p_O - p_s)}{g} \tag{2}$$

$$m_{char} = \frac{A(p_D - p_s)}{g} \tag{3}$$

here, g is the accerelation due to gravity and A is the cross-sectional area of the bed. For the same air flowrate, p_s is the pressure drop in the bed containing only the sand particles, p_O is the peak pressure drop after the biomass is introduced and p_D is the pressure drop recorded at the end of devolatilization. Substituting Eqs. (2) and (3) in Eq. (1), the char yield can be measured from

$$\gamma_{char} = \frac{p_D - p_s}{p_O - p_s} \tag{4}$$

The mean pressure drop in the pure sand bed is shown in Fig. 4(a) for the range of air flowrates used in this study. The error bar indicates the standard deviation of the mean pressure over the 120 s measurement interval. As shown in the figure, the pressure drop is close to the bed weight per unit area, indicating that the bed is in fluidized state at each air flowrate.

Due to the bed fluctuation, it will be difficult to obtain the pressures at points **O** and **D** directly from the pressure curve. It should be noted that the required values of p_D and p_O are at the indicated time instances unlike the pressure drop in the pure sand bed that is measured as an average value over a time interval with measurement uncertainty σ_s^2, where σ_s is the standard deviation of the measurement. For the bed containing biomass, a linear line drawn through point **O** and **D** is introduced as shown in Fig. 4(b). From the line, an average pressure drop

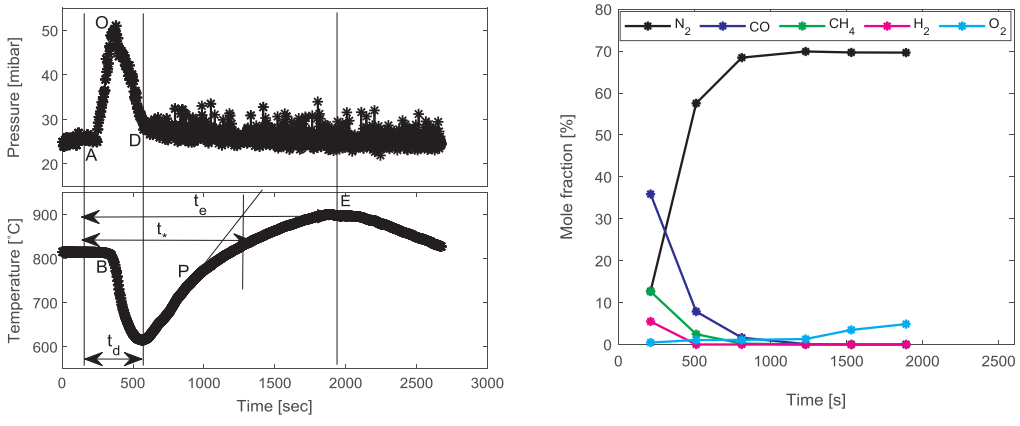

(a) (b)

Fig. 2. Phases of biomass conversion in a bubbling bed containing 26.4 vol% wood pellets at air flowrate of 1.0 kg/h (a) pressure drop and temperature (b) composition of the product gas.

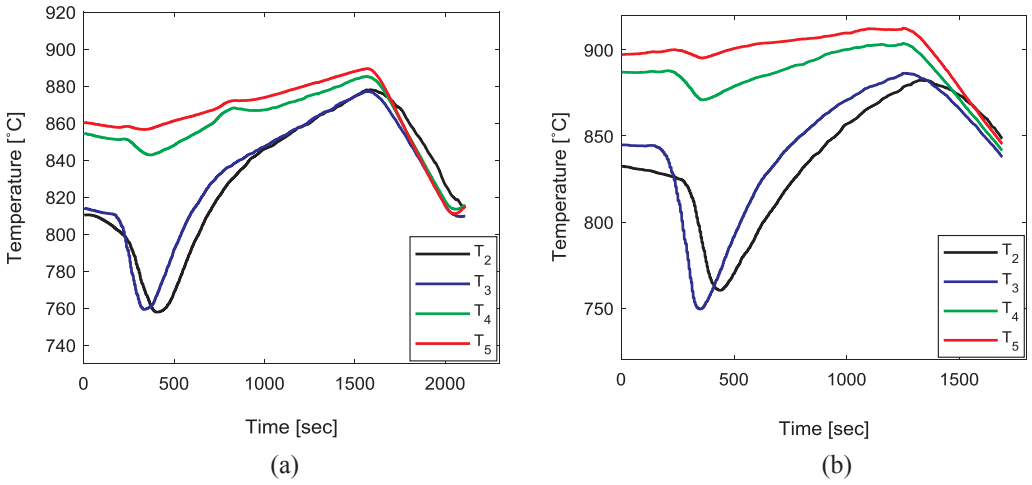

Fig. 3. Temperature variation along the reactor axis for two different beds at 1.2 kg/h air flowrate (a) 20.2 vol% wood pellets (b) 21.3 vol% wood chips.

at a given time between **O** and **D** can be approximately estimated. Assuming that the variance is uniformly distributed over the measurement interval, the uncertainty σ_p^2 in the pressure drop measurement can be computed from

$$\sigma_p^2 = \left(\sqrt{\frac{1}{N} \sum_i (p_i - \bar{p_i})^2} - \sigma_s \right)^2 \tag{5}$$

here, $\bar{p_i}$ is the pressure drop estimated from the linear model and p_i is the actual pressure drop measured at the same time. Applying the differential method, the uncertainty σ_{char}^2 in the measurement of the char yield can be determined from

$$\sigma_{char}^2 = \left(\frac{\partial \gamma_{char}}{\partial p_D} \right)^2 \sigma_p^2 + \left(\frac{\partial \gamma_{char}}{\partial p_O} \right)^2 \sigma_p^2 \tag{6}$$

which leads to

$$\frac{\sigma_{char}^2}{\gamma_{char}^2} = \left[\frac{1}{(\bar{p_D} - p_s)^2} + \frac{1}{(\bar{p_O} - p_s)^2} \right] \sigma_p^2 \tag{7}$$

At the completion of the devolatilization, the total heat loss Q_L can be obtained from the difference between the heat content of the bed before the temperature begins to drop significantly and the heat content at the end of the devolatilization as expressed below

$$Q_L = -m_S c_{p,S} (T_D - T_B) \tag{8}$$

where T_B is the bed temperature before the significant drop is observed and T_D is the temperature at the completion of devolatilization. m_S is the total mass of solid between point **B** and **D** neglecting the mass loss and $c_{p,S}$ is the specific heat capacity of the bed. It should be noted that Q_L is the net heat loss in the bed, which also accounts for the sensible heat loss by the flowing gas and the heat loss through the reactor walls. Dividing Eq. (8) through with $m_S c_{p,S}(t_D - t_B)$, the specific rate of heat loss $\dot{q}_L$, can then be obtained as

$$\dot{q}_L = \frac{T_B - T_D}{t_D - t_B} \tag{9}$$

Since the value of $\dot{q}_L$ determined from Eq. (9) may change along the bed axis as can be seen in Fig. 3, the average value between points 2 and 3 in the bed is computed and recorded for each experimental run.

3. Results and discussion

The analysis and results of the experimental data from conversion of the five different biomass loads at different air flowrates are presented in this section. Fig. 5 shows the temperature curve for the bed containing 20.2 vol% wood pellets compared to that of wood chips of approximately equal volume at the same air flowrate, 1.5 kg/h. It should be noted that on an equal volume basis, the two different beds contain approximately the same number of biomass particles. However, on the basis of equal mass, the difference between the hydrodynamic behaviour of the two different beds will be very large since the number of

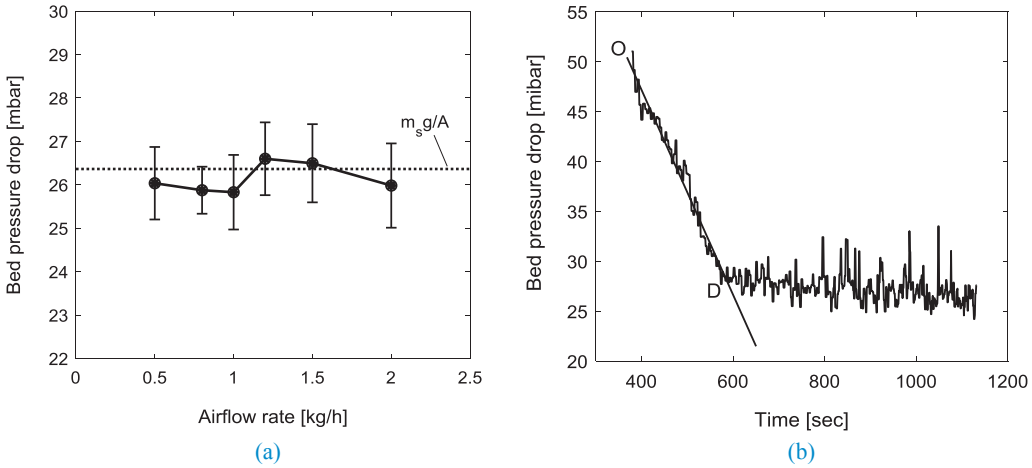

Fig. 4. (a) Pressure drop in the bed of pure 293 μm sand particles at 830 ± 20 °C and different air flowrates (b) linear model illustrating the measurement of pressure drops at points **O** and **D** in a bed containing biomass.

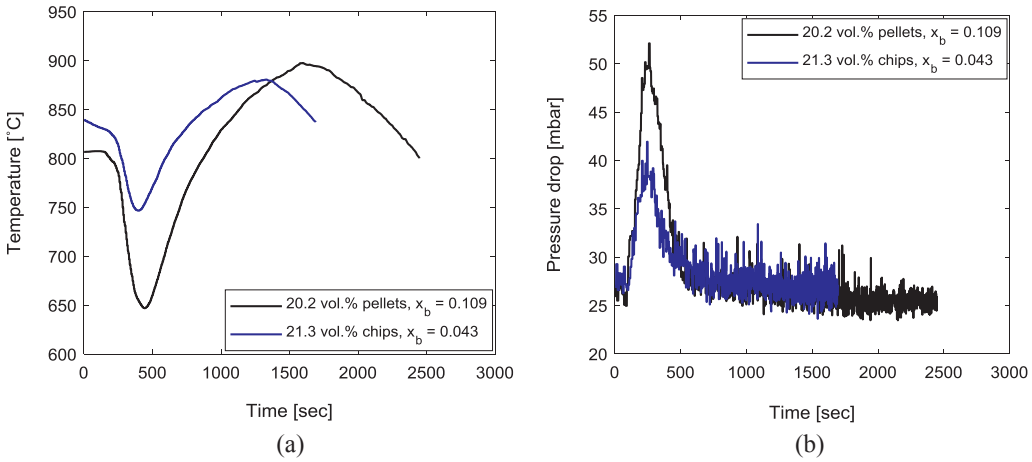

Fig. 5. (a) Temperature curves in the bed of wood chips (21.3 vol%) and pellets (20.2 vol%) at 14.3 cm from the bed base and air flowrate of 1.5 kg/h (b) pressure drops over the two different beds.

biomass particles in the bed of wood chips will be approximately three times as large as that in the pellet bed. Although the trends in Fig. 5(a) are similar for both beds, the results show that the initial mass fraction of biomass in the bed influences the extent to which the bed transits from one stage to another as discussed in Section 2.2. Due to higher mass percentage, the temperature drop during the heating up and devolatilization is higher in the bed with wood pellets. Both the devolatilization and extinction times are also higher in the pellet bed. The peak bed temperature is higher in the bed with pellets due to larger amount of char present after the time, t_d compared to the amount present in the bed with wood chips. Moreover, the peak pressure in the wood chip bed is lower due to the smaller biomass mass load compared to that of the pellet bed as shown in Fig. 5(b).

3.1. Devolatilization and char residence times

Fig. 6 shows the variation of the residence times with the applied air flowrate at different biomass loads. The char residence time, $(t_e - t_d)$ is considerably higher than the corresponding value of t_d at a given gas flowrate in both types of biomass. Both values of $(t_e - t_d)$ and t_d decrease with an increase in air flowrate. As the two biomass loads, x_b for the wood chips are lower than those of the pellets, it is clear that at the same air flowrate, the corresponding residence time increases with increasing amount of biomass in the bed despite the biomass type. However, the dependency of the devolatilization time on the value of x_b is less clear as can be seen in the figures.

3.2. Char yield and heat loss at completion of devolatilization

The amount of unconverted biomass, γ_{char} at the completion of devolatilization is shown in Fig. 7(a) as a function of initial biomass load and air flowrates. The error bar represents the uncertainty σ^2_{char} in the measurement where the mean value over the 29 experimental runs is $\pm$ 8.8x10^{-4}. For both types of biomass, the value of γ_{char} decreases with an increase in air flowrate and a decrease in the value of x_b. As shown in Fig. 7(b), the heat loss increases with increasing air flowrate and biomass load owing to the increasing sensible heat loss from the larger mass flowrate of gas and larger amount of cold biomass introduced in the bed. With a higher heat loss, the final temperature at the completion of devolatilization decreases, resulting in a higher char yield. However, with an increase in air flowrate, partial oxidation of the char particles is enhanced due to higher availability of oxygen. This thus decreases the char yield at increasing air flowrate even though the heat loss is increased.

3.3. Correlations of the experimental data

As discussed above, the characteristic residence time depends on the air flowrate and the initial amount of biomass in the bed. The reaction time parameters are important for ensuring efficient conversion of biomass, particularly during the gasification process. Correlating the data obtained in this study can be useful when scaling up the bed. For the behaviour to be applied to larger beds, the flow variables need to be

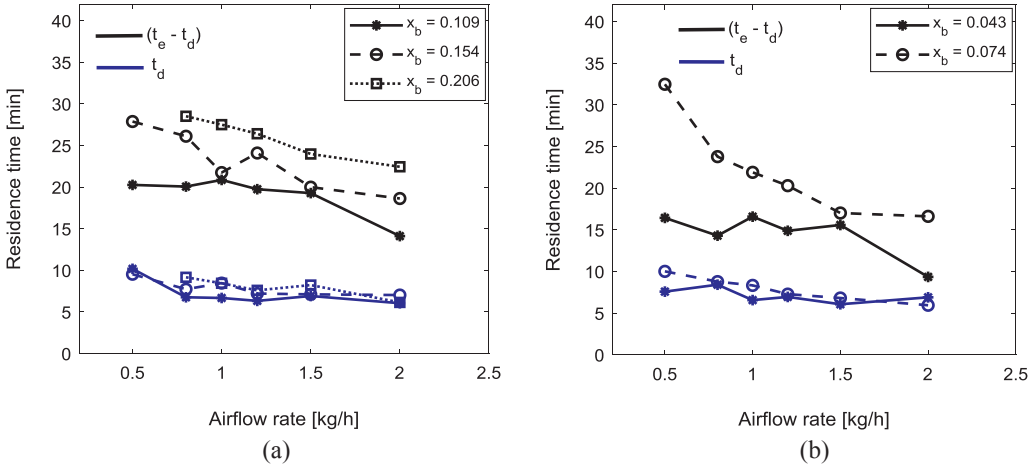

Fig. 6. Comparison between the devolatilization time and char residence time at different biomass loads (a) wood pellets (b) wood chips.

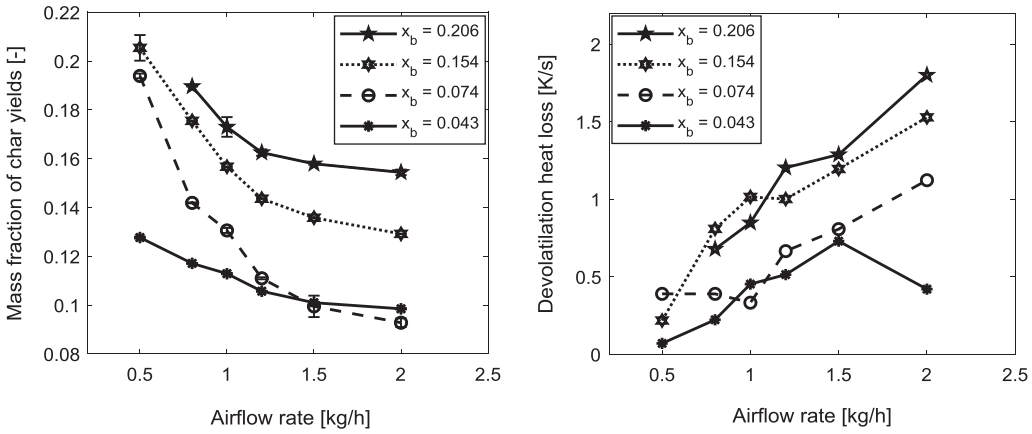

Fig. 7. Effect of biomass load and air flowrate on the biomass devolatilization (a) char yield (b) heat loss.

scaled in a similar manner to the amount of biomass added in the bed. The effect of the bed material needs to be considered also since the degree of fluidization at a given air flowrate depends on the particle properties (size, shape and density). To correctly scale the bed behaviour, the values of t_d and t_e are compared at different values of x_b and U_0/U_{mf}, where $U_0 = \dot{m}_{air}/(\rho_{air}A)$ is the superficial air velocity for a given air flowrate $\dot{m}_{air}$, and U_{mf} is the minimum fluidization velocity of the bed material at the operating conditions.

Fig. 8(a) shows the plot of $\log_{10}(x_b^a t_d)$ against $\log_{10}(U_0/U_{mf})$ while the corresponding plot for the value of t_e is shown in Fig. 8(b). With reference to the points **D** and **E** shown in Fig. 2, the value ofU_0 at each air flowrate is obtained at the temperature corresponding to the respective points while the corresponding value of U_{mf} is predicted using the Wen and Yu [32] correlation. For each plot in Fig. 8, the value of a is obtained by minimizing the mean square error between the fitting line and the experimental data. The results show that both values of $\log_{10}(x_b^a t_d)$ and $\log_{10}(x_b^a t_e)$ decrease linearly with increasing value of $\log_{10}(U_0/U_{mf})$ with correlation coefficients (R^2-values) of 0.64 and 0.73, respectively. Thus, from the fitting lines, t_d [min] and t_e [min] can be modelled as

$$t_d = 11.35 x_b^{0.028}\left(\frac{U_0}{U_{mf}}\right)^{-0.3} \tag{10}$$

$$t_e = 67.58 x_b^{0.278}\left(\frac{U_0}{U_{mf}}\right)^{-0.185} \tag{11}$$

The accuracies of the models described by Eqs. (10) and (11) are demonstrated in Fig. 9. Fig. 9(a) and Fig. 9(b) display the calculated versus the measured biomass residence time for the devolatilization and char extinction, respectively. As can be seen, the uncertainties in the model predictions are ± 10% for both t_d and t_e, where the mean absolute errors are 7.7% and 7.6%, respectively. The higher range of errors are still within acceptable limits for initial design phase and validation of CFD models.

Similarly, Eqs (12) and (13) give the correlations of the char yields and heat losses at different biomass loads and air flowrates. The overall error in the prediction of γ_{char} includes the uncertainty in the experimental data as described in Section 2.3. Both equations can be applied in modelling an air-biomass gasification process to account for the initial char yield and heat loss during the devolatilization.

$$\gamma_{char} = 0.414 x_b^{0.245}\left(\frac{U_0}{U_{mf}}\right)^{-0.463} \pm 18\% \tag{12}$$

$$\dot{q}_L = 1.664\left(\frac{U_0}{U_{mf}} x_b\right)^{0.767} \pm 25\% \tag{13}$$

3.4. Application to a continuous gasification process

To apply Eqs. (12) and (13) to a continuous process, the biomass load x_b in the bed at the given operating conditions is required. As an approximation, a plug flow process can be considered over a cycle period, t_e at the given biomass and air flowrates. By plug flow, it is assumed that all particles have the same residence time thereby reducing the instability that arises due to gas flow [33,34]. Given a constant mass flow of biomass $\dot{m}_b$ and a fixed mass of the bed material, m_p, the

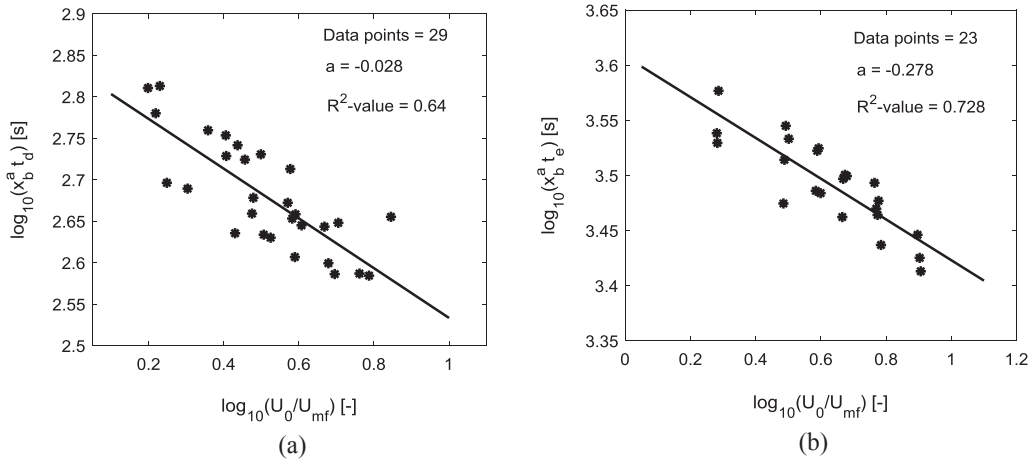

Fig. 8. Correlation of the characteristic residence time for biomass conversion (a) devolatilization (b) extinction.

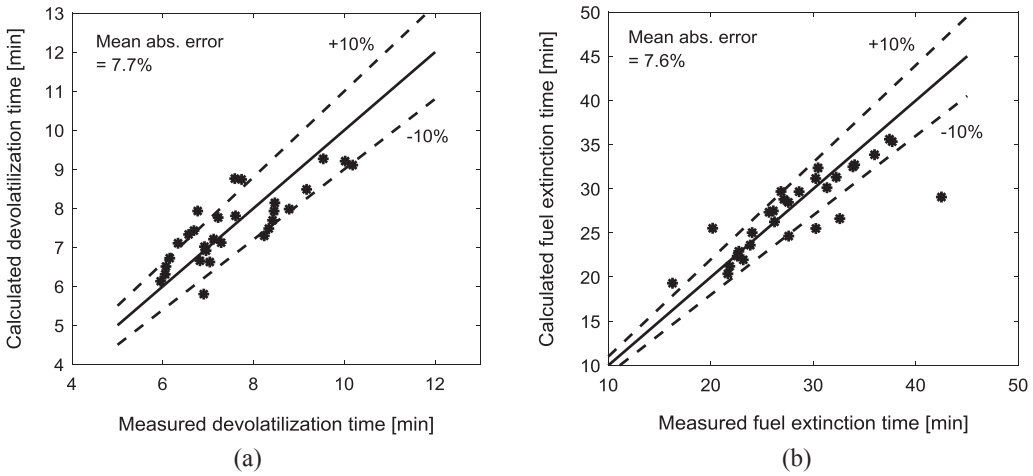

Fig. 9. Computed versus measured biomass characteristic residence time (a) devolatilization (b) extinction, showing the accuracy of the models given by Eqs. (10) and (11), respectively. The experimental data are those obtained in this study from the five different biomass loads at the six different air flowrates for each load.

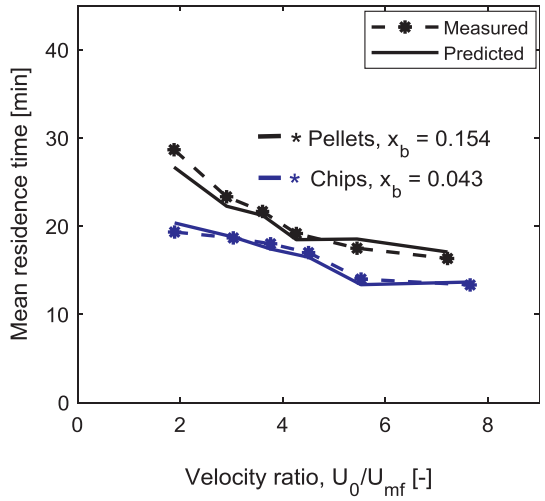

Fig. 10. Biomass mean residence time comparing the predicted results with the measured data.

value of x_b can be obtained from the following expression derived from Eq. (11).

$$x_b = \left[4055\frac{\dot{m}_b}{m_p}\left(\frac{U_0}{U_{mf}}\right)^{-0.185}\right]^{1.385} \tag{14}$$

Moreover, $(t_e - t_d)/t_d > 1.0$ at any given biomass load and air flowrate as shown in Fig. 6. For a continuous flow of biomass in a bubbling fluidized bed, this means that there will be excessive pressure build-up due to biomass accumulation when the residence time of the fuel particles is in the order of t_d. To obtain a stable process where the pressure in the bed is relatively low over an operating period, the biomass residence time must lie between t_d and t_e. Supposing t_* is the operating mean residence time, the degree of char conversion or reaction completeness α can be obtained as

$$\alpha = \frac{t_* - t_d}{t_e - t_d} \tag{15}$$

The value of α ranges from 0 to 1. When $\alpha = 0$, the amount of char in the bed grows at the rate γ_{char} kg/kg raw biomass and no steady state can be attained, although the product gas will be rich in combustible gases. When $\alpha = 1$, the biomass particles in the bed will be reduced to approximately zero, and the exit gas will contain, beside nitrogen and unconverted oxygen, mostly CO_2 and H_2O. However, by assessing the

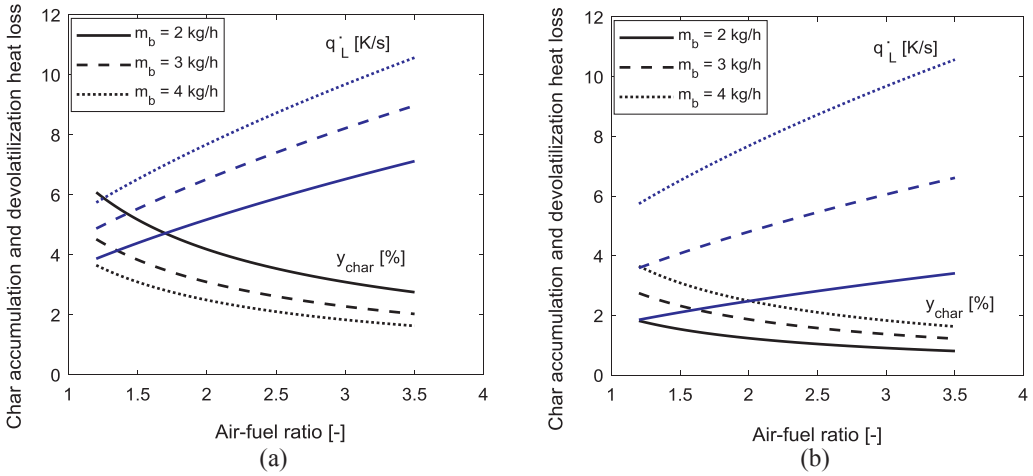

Fig. 11. Computed amount of accumulated char particles based on Eq. (17) and heat loss based on Eq. (13) in a bubbling fluidized bed for a continuous flow of biomass, showing the effect of bed solid loading ratio at different air–fuel ratios (a) constant biomass flowrate to bed material mass ratio $\dot{m}_b/m_p = 1.0$ 1/h (b) constant bed material mass $m_p = 4$ kg. $T = 800$ ℃, bed particle size = 300 μm and the bed diameter = 0.15 m.

temperature profile for a typical biomass conversion as shown in Fig. 2, it is clear that $0 < \alpha < 1$ will always be true for any given continuous process. The operating value of α can be taken as that corresponding to the mean residence time t_* as indicated in Fig. 2. The analysis shows that α varies within 0.45–0.7 for both types of biomass. The mean value of α for the wood pellets is 0.55 while that for the wood chips is 0.6.

Fig. 10 compares the mean residence time, t_* obtained as described in Fig. 2 with the values predicted using a combination of Eq. (10), Eq. (11) and the conversion factor α for different biomass loads. The superficial air velocity U_0 and the minimum fluidization velocity U_{mf} of the 293 μm sand particles are evaluated at the temperature measured at the time, $t = t_*$ during the conversion period, and the value of α is based on the value corresponding to each air flowrate in the respective beds. As can be seen in Fig. 10, the computed values of t_* are closer to the measured values, despite the temperature difference at the devolatilization and extinction times, t_d and t_e. This therefore shows that for subsequent applications, the values of t_d and t_e can be obtained at the given bed operating temperature.

Based on the degree of conversion, the amount of unconverted char particles x_{char} within the period $(t_e - t_d)$ can be thus predicted from

$$x_{char} = (1 - \alpha)\gamma_{char}(t_e - t_d)\frac{\dot{m}_b}{m_p} \tag{16}$$

where x_{char} is the mass ratio of the unconverted char to the bed material. t_d and t_e can be computed using Eqs. (10) and (11). As a percentage y_{char} of the total solids in the bed, Eq. (16) can be re-expressed as

$$y_{char} = \frac{x_{char}}{x_{char} + 1}100\% \tag{17}$$

Using the value of y_{char} estimated from Eq. (17), the minimum fluidization velocity, the minimum slugging velocity and other bubble-induced properties in a biomass bubbling fluidized bed gasifier can be predicted. In addition, with the value of x_{char}, the solids circulation rate, $\dot{m}_{sc}$ required for a dual fluidized-bed biomass gasifier can also be determined as described below:

$$\dot{m}_{sc} = \frac{m_p}{(1 - \alpha)(t_e - t_d)}(x_{char} + 1) \tag{18}$$

Although dual fluidized-bed gasifiers are originally operated for steam-biomass gasification [1], applying this technology in an air-blown gasifier can also help to achieve gasification at low air–fuel ratios, thereby achieving higher CO and H_2 yields in the syngas as for a single bubbling or circulating fluidized bed under autothermal operation (air-blown).

The application of the above correlations in a continuous biomass gasification process is illustrated in Fig. 11. For the same biomass and air flowrates, the figure compares the values of $\dot{q}_L$ and y_{char} at different loadings of the bed material. The mass loading ratio $\dot{m}_b/m_p = 1.0\ \mathrm{h}^{-1}$ is constant in Fig. 11(a), giving different values of m_p at different biomass feeds, while in Fig. 11(b), the mass of the bed material $m_p = 4$ kg is constant. The gasification temperature is 800 ˚C, the particle size is 300 μm and the degree of conversion $\alpha = 0.6$ in all the plots. With an increase in the air–fuel ratio at the same biomass flowrate, the relative amount of char accumulated in the bed decreases and the heat loss during the devolatilization increases due to the increase in gas velocity, U_0/U_{mf}. The figures also show that the value of $\dot{q}_L$ increases with increasing biomass feed rate. At the constant mass load ratio, the char accumulation decreases with increasing biomass flowrate due to the increasing mass of the bed material. Comparing Fig. 11(a) and (b), it can be seen that the heat loss decreases as the mass of the bed material increases, which can be connected to the increasing heat-holding capacity of the bed. With the lower heat loss, the char yield decreases, which can also explain the increasing char accumulation shown in Fig. 11(b) as the biomass supply increases.

In addition to air–fuel ratio, the results described above show that the gas velocity ratio U_0/U_{mf} is an important parameter that influences the extent of biomass conversion in a fluidized bed. Since the rates of particle entrainment and elutriation also depend on U_0/U_{mf} and on the amount of char present, the gas velocity ratio must be selected with caution for successful operation of a fluidized bed gasifier. Moreover, the value of x_{char} obtained from the proposed model is not a steady state value at the given biomass flowrate and gasification conditions since it is based on t_e, a time value very small to achieve a steady state in a gasifier. As shown in Timmer and Brown [4], it can take over 12 h for a steady state condition to be achieved under elutriation effect. Without particle elutriation, this condition will take several more hours if it exists. The value of t_e can be larger than 20 min, which is sufficiently long for successful control of a biomass gasification process. In addition, the proposed model for x_{char} is developed based on the ideal plug flow which gives the desirable flow pattern for any continuous fluidized bed [33,34]. Hence, Eq. (16) gives a more reliable information for successful design and operation of a bubbling fluidized bed gasifier than any steady state value.

4. Conclusions

This study presented a method for obtaining the residence time required for complete conversion of biomass in a bubbling fluidized bed using the time-variation of temperature and pressure in the bed. At any given biomass load and air flowrate, two characteristic times described as devolatilization and extinction times, were observed. The devolatilization time denotes the end of the conversion phase below which the exit gas contains combustible gases such as CO, H_2 and CH_4 while the extinction time marks the time over which nearly all the biomass charged in the bed is completely consumed. Both characteristic times decrease with increasing air flowrate and decreasing initial amount of biomass in the bed. In addition, the amount of char released and the total heat loss during the devolatilization were also measured and characterized.

Based on the data obtained in this study, different correlations were proposed for estimation of the mean biomass residence time, the amount of unconverted char particles and the devolatilization heat loss at a given operating condition. The prediction of the amount of biomass accumulated in the bed can be used in determining the minimum fluidization velocity, slugging velocity and other bubble-induced bed properties as well as the solids circulation rate desired for decongesting the accumulated biomass particles. The developed tools can provide a fast and accurate prediction of fluidized bed behaviour for biomass gasification.

Funding sources

This research did not receive any specific grant from funding agencies in the public, commercial, or not-for-profit sectors.

References

[1] Corella J, Toledo JM, Molina G. A review on dual fluidized-bed biomass gasifiers. Ind Eng Chem Res 2007;46:6831.
[2] Zou Z, Zhao Y-L, Zhao H, Zhang L-B, Xie Z-H, Li H-Z, et al. Hydrodynamic and solids residence time distribution in a binary bubbling fluidized bed: 3D computational study coupled with the structure-based drag model. Chem Eng J 2017;321:184.
[3] Ghaly AE, MacDonald KN. Mixing patterns and residence time determination in a bubbling fluidized bed system. Am J Eng Appl Sci 2012;5:170.
[4] Timmer KJ, Brown RC. Transformation of char carbon during bubbling fluidized bed gasification of biomass. Fuel 2019;242:837.
[5] Di Renzo A, Di Maio FP, Girimonte R, Vivacqua V. Segregation direction reversal of gas-fluidized biomass/inert mixtures – experiments based on Particle Segregation Model predictions. Chem Eng J 2015;262:727.
[6] Goldschmidt MJV, Link JM, Mellema S, Kuipers JAM. Digital image analysis measurements of bed expansion and segregation dynamics in dense gas-fluidized beds. Powder Technol 2003;138:135.
[7] Fiorentino M, Marzocchella A, Salatino P. Segregation of fuel particles and volatile matter during devolatilization in a fluidized bed reactor – II. Experimental. Chem Eng Sci 1909;1997:52.
[8] Solimene R, Marzocchella A, Salatino P. Hydrodynamic interaction between a

coarse gas-emitting particle and a gas fluidized bed of finer solids. Powder Technol 2003;133:79.
[9] Werther J, Hirschberg B. Solids motion and mixing. In: Grace JR, Avidan AA, Knowlton TM, editors. Circulating fluidized bed. London: Chapman and Hall; 1997. p. 119–48.
[10] Gao W, Zhang J, Wang Y, Huang B, Xu G. Residence time distribution of particles in a bubbling fluidized bed with their continuous input and output. Chin J Process Eng 2012;12:9.
[11] Li XT, Grace JR, Lim CJ, Watkinson AP, Chen HP, Kim JR. Biomass gasification in a circulating fluidized bed. Biomass Bioenergy 2004;26:171.
[12] Gomez-Barea A, Arjona R, Ollero P. Pilot-plant gasification of olive stone: a technical assessment. Energy Fuels 2005;19:598.
[13] Lv PM, Xiong ZH, Chang J, Wu CZ, Chen Y, Zhu JX. An experimental study on biomass air-steam gasification in a fluidized bed. Bioresour Technol 2004;95:95.
[14] Brown RC, Ahrens J, Christofides N. The contributions of attrition and fragmentation to char elutriation from fluidized beds. Combust Flame 1992;89:95.
[15] Gaston KR, Jarvis MW, Pepiot P, Smith Jr. KM, Frederick WJ, Nimlos MR. Biomass pyrolysis and gasification of varying particles sizes in a fluidized-bed reactor. Energy Fuels 2011;25:3747.
[16] Zanzi R, Sjostrom K, Bjornbom E. Rapid pyrolysis of agricultural residues at high temperature. Biomass Energy 2002;23:357.
[17] Zanzi R, Sjostrom K, Bjornbom E. Rapid high-temperature pyrolysis of biomass in a free-fall reactor. Fuel 1996;75:545.
[18] Mathieu P, Dubuisson R. Performance analysis of a biomass gasifier. Energy Convers Manage 2002;43:1291.
[19] Scott DS, Piskorz J, Bergougnou MA, Graham R, Overend RP. Role of temperature in the fast pyrolysis of cellulose and wood. Ind Eng Chem Res 1988;27:8.
[20] Gable P, Brown RC. Effect of biomass heating time on bio-oil yields in a free fall fast pyrolysis reactor. Fuel 2016;166:361.
[21] Bar-Ziv E, Kantorovich II. Mutual effects of porosity and reactivity in char oxidation. Prog Energy Combust Sci 2001;27:667.
[22] Henrich E, Buerkle S, Meza-Renken ZI, Rumpel S. Combustion and gasification kinetics of pyrolysis chars from waste and biomass. J Anal Appl Pyrol 1999;49:221.
[23] Wornat MJ, Hurt RH, Yang NYC, Headley TJ. Structural and compositional transformations of biomass chars during combustion. Combust Flame 1995;100:131.
[24] Paudel B, Feng Z-G. Prediction of minimum fluidization velocity for binary mixtures of biomass and inert particles. Powder Technol 2013;237:134.
[25] Kumoro AC, Nasution DA, Cifriadi A, Purbasari A, Falaah AF. A new correlation for the prediction of minimum fluidization of sand and irregularly shape biomass mixtures in a bubbling fluidized bed. IJAER 2014;9:21561.
[26] Agu CE, Tokheim L-A, Eikeland M, Moldestad BME. Improved models for predicting bubble velocity, bubble frequency and bed expansion in a bubbling fluidized bed. Chem Eng Res Des 2019;141:361.
[27] Viitanen PI. Tracer studies on a riser reactor of a fluidised catalytic cracking plant. Ind Eng Chem Res 1993;32:577.
[28] Helmrich H, Schugerl K, Janssen K. Decomposition of $NaHCO_3$ in laboratory and bench scale circulating fluidized bed reactors. In: Basu P, editor. Circulating fluidized bed technology. New York: Pergamon Press; 1985. p. 161–6.
[29] Kojima T, Ishihara K, Guilin Y, Furusawa T. Measurement of solids behaviour in a fast fluidised bed. J Chem Eng Jpn 1989;22:341.
[30] Xu R, Ferrante L, Briens C, Berruti F. Bio-oil production by flash pyrolysis of sugarcane residues and post treatments of the aqueous phase. J Anal Appl Pyrol 2011;91:263.
[31] Tran HC, White RH. Burning rate of solid wood measured in a heat release rate calorimeter. Fire Mater 1992;16:197.
[32] Wen CY, Yu YH. A generalized method for predicting the minimum fluidization velocity. AIChE J 1966;12:610.
[33] Chandran AN, Rao SS, Varma YBG. Fluidized bed drying of solids. AIChE J 1990;36:29.
[34] Raghuraman J, Varma YBG. An experimental investigation of the residence time distribution of solids in multistage fluidisation. Chem Eng Sci 1975;30:145.